RAPID COMMUNICATIONS IN MASS SPECTROMETRY, VOL. 10, 691–698 (1996)

Thermodynamic and Phase Diagram Studies on Metal–Tellurium Systems Employing Knudsen Effusion Mass Spectrometry

Magapu Sai Baba,* Radhakrishnan Viswanathan and Cherian K. Mathews

Materials Chemistry Division, Chemical Group, Indira Gandhi Centre for Atomic Research, Kalapakkam-603 102, Tamil Nadu, India

SPONSOR REFEREE: Professor D. Mathur, Tata Institute of Fundamental Research, Bombay, India.

Reliable thermodynamic and phase diagram data are essential to understand the behaviour of fuels in a nuclear reactor. The fission product tellurium is believed to play a significant role in fuel–cladding interaction in the oxide-fuelled fast breeder reactor. In order to assess its role in the fuel–cladding interaction, a systematic study of the binary systems of Te and a cladding component (Fe, Cr, Ni, Mo and Mn) was taken up in our laboratory. The Knudsen effusion mass spectrometric technique was employed very effectively to obtain both thermodynamic and phase diagram information. This paper summarizes the results obtained from these studies. Most of these tellurides exhibit non stoichiometry. Making use of the property of preferential evaporation of one of the components from these metal tellurides, the homogeneity ranges of most of these phases were determined. The thermodynamic data determined were employed to calculate the threshold tellurium potential required for the formation of metal tellurides from the fuel-cladding interaction and compared with the equilibrium tellurium potential that is likely to be present in the fuel–cladding gap in a fast breeder reactor.

In a fast breeder reactor, energy is produced by nuclear fission induced by fast neutrons. A mixed uranium–plutonium oxide is generally used as a fuel and 316 stainless steel or its stabilized varieties as cladding material. During the reactor operation, the cladding tube experiences a hostile, fission-product environment at high temperatures which may lead to several types of interactions. A host of thermodynamic data are needed to understand the various phenomena that occur in a nuclear reactor. For example, an assessment of fuel–cladding, fuel–coolant and fuel–fission product interactions is essential to understand fuel behaviour in operating and off-normal conditions. Often it is the fuel–cladding interaction that governs the performance of the fuel and restricts the extended use of the fuel in a reactor. It is believed that the fission product tellurium plays a significant role in fuel–cladding interaction in fast breeder reactor fuels.[1] In order to assess the role played by tellurium in the fuel–cladding interaction, it is necessary to generate thermodynamic data on tellurides of cladding components. As most of the cladding component tellurides exhibit non stoichiometry, it is also necessary to determine the homogeneity ranges of these phases. A systematic study of the thermodynamic and phase diagram properties of transition metal–tellurium systems, employing Knudsen effusion mass spectrometry was taken up in our laboratory. In this paper we summarize the results obtained on the binary systems of a cladding component (Fe, Ni, CR, Mo and Mn) with Te. By employing the thermodynamic data thus generated, the threshold tellurium potentials required for the formation of these tellurides from stainless steel cladding are calculated and compared with the equilibrium tellurium potential that is likely to exist in the fuel–cladding gap. Details of our studies on individual binary systems Fe–Te,[2,3] Ni–Te,[4] Cr–Te[5,6] Mo–Te[7,8] and Mn–Te[9] are found elsewhere.

A mass spectrometer coupled to a Knudsen effusion vapour source offers a unique opportunity to study both gas phase and gas–solid (or gas–liquid) equilibria. In this method, the vapour in equilibrium with one or more condensed phases (either solid or liquid) is sampled, without disturbing the equilibrium conditions, ionized in an ion source (generally an electron ionization source) and the ions mass analysed and detected by using either an electron multiplier and/or a Faraday cup. An electron ionization source in which electron energy can be varied, enables one to measure the intensities of various ions as a function of electron energy and therefore derive appearance energies. Gas phase processes such as fragmentation, dissociation etc., can be studied with ease. As equilibrium vapour is sampled from the Knudsen effusion cell, it also enables one to study equilibrium properties (partial pressure etc.) and arrive at thermodynamic information on the condensed phase (such as the enthalpy, entropy, etc.). Knudsen effusion mass spectrometry has been employed very effectively for both these purposes. Excellent reviews are available on this topic in the literature.[10–13]

EXPERIMENTAL

Vaporization studies were conducted by using a VG Micromass 30 BK mass spectrometer. The molecular beam effusing out of a Knudsen cell was ionized by electron ionization. The ionizing electron beam was set at an emission current (trap+source) of 100 μA. The positive ions thus produced were accelerated to a potential of 6 kV and subsequently mass analysed by a 90° sector, 30 cm radius, single focusing magnetic analyser. A pneumatically-controlled shutter was placed between the effusing molecular beam and the electron ionization source, thus making it possible to differentiate between ions produced from the sample and those from the background gases present in the ion source. Ion currents were measured by a secondary electron multiplier. Data acquisition and processing were carried out using an IBM-compatible PC.

Samples were contained in alumina Knudsen cells (i.d. 7.5 mm; o.d. 10.0 mm; height 10.0 mm; orifice diameter

* Author for correspondence.

CCC 0951–4198/96/060691–08

Received 31 January 1996
Accepted 12 February 1996

0.5 mm) kept inside a molybdenum or tantalum chamber which was heated by electron bombardment. Sample temperatures were measured by a chromel–alumel thermocouple touching the base of the Knudsen cell. This was calibrated against the melting point of silver. The first ionization energies in In^+, Ag^+, Hg^+, Ar^+ and He^+ were used to calibrate the electron energy scale. Both calibrations, of the thermocouple and the electron energy scale, were carried out periodically to verify the validity of the calibration (see references 4, 14 and 15 for more details.

The Knudsen effusion mass spectrometer has been modified extensively by us. The originally purchased two-in-one mass spectrometer was separated into two independently operating thermal ionization and Knudsen effusion mass spectrometers. The electron bombardment furnace used for heating the Knudsen cell supplied by the manufacturer has been replaced with a home-built furnace.[16] The power supply and temperature control panels of the electron bombardment furnace were also modified, which resulted in better control of the temperature of the Knudsen cell. Similarly the outdated HP-9830A programmable calculator used for instrument control and data acquisition was replaced by an IBM-compatible PC. The necessary software required for the data acquisition and treatment was developed in-house. These changes are described in some detail in References 17 and 18.

Samples for each of the vaporization experiments consisted of a two-phase mixture of either, $(M+MTe_x)$ where M=Fe, Ni, Cr, Mo and Mn[2, 4, 5, 7, 9] or (MTe_x+MTe_y) where M=Fe[3] and Mo.[8] In the case of studies with Cr–Te alloys, samples belonging to the phase-field $CrTe_{1-x}$ and $(CrTe_x+Te)$ were also prepared.[6] The samples were prepared by heating thoroughly-ground mixtures of appropriate amounts of the respective elements contained in evacuated sealed quartz tubes. The phases formed at the end of the heating were characterized by x-ray diffraction.

The species present in the mass spectrum of the equilibrium vapour were identified by their masses and isotopic abundances. Ionization efficiency curves were obtained by recording ion intensity variation as a function of electron energy at constant sample temperature. Appearance energies were deduced from the ionization efficiency curves by the method of linear extrapolation. Whether the ions detected were formed due to simple ionization or fragmentation was determined from their appearance energies.

Methodology

The experiments carried out in the study of the vaporization behaviour of metal–tellurium systems can be divided into two types. In the first type, temperature dependence of ion intensities was obtained. In the second type, homogeneity ranges of the non-stoichiometric metal telluride phases were obtained. From the temperature dependence of ion intensities, relations between partial pressure and temperature were deduced. A brief description of the procedure adopted in the two cases is given below.

Determination of partial pressures

The ion intensity, I_i, corresponding to species i, can be related to its partial pressure, p_i, by using the following expression

$$p_i = kIT/(\sigma s h)_i \quad (1)$$

where σ is the ionization cross-section, s the multiplier response, h the isotopic abundance of species 'i', T is the temperature, and k the instrument calibration constant.[11] In most cases, the instrument calibration constant was obtained by performing vaporization experiments with elemental tellurium, both before and after each of the vaporization experiments with metal–tellurium systems. Such a choice avoids the use of actual values for the ionization cross section and this and all the other constants get absorbed into the constant k' (where $k'=k/\sigma sh$). For obtaining the partial pressure of other species, the constant k' was corrected for the change in the values of σ, s and h. The multiplier response (s) was taken to be inversely proportional to the square root of the mass. The isotopic abundance (h) for molecules was calculated from the isotopic abundances of constituent elements.

Determination of homogeneity range

Most of these tellurides were found to preferentially vaporize as tellurium. This property was made use of to obtain the homogeneity ranges of the non-stoichiometric telluride phases. The starting compositions of the samples in such experiments were chosen to be tellurium-rich two-phase mixtures. The samples were heated to a particular temperature and the ion intensities were monitored as a function of time throughout the period of vaporization. Since tellurium is preferentially lost from the two-phase mixture, the condensed phase becomes depleted in tellurium. However, the ion intensities remain constant so long as the sample remains in a two-phase mixture and only start decreasing once the sample enters into the single-phase region. The ion intensities attain constancy once the condensed-phase composition changes to that of a new two-phase mixture. The total mass loss in each experiment was obtained by weighing the sample before and after each experiment. By correlating the initial weight, initial composition, total mass loss and the integrated ion currents, the phase-boundary composition could be arrived at with the help of the equations given below.

The Hertz–Knudsen equation[10] relates the mass loss to the partial pressure

$$\Delta W_i = p_i[M_i/2\pi RT]^{1/2} taC \quad (2)$$

where Δw_i is the mass loss of the condensed phase due to effusion of a gaseous species i of molar mass M_i, p_i is the partial pressure of the species at temperature T, t is the time, a is the orifice area and C is the Clausing factor for the orifice. When the vapour phase consists of more than one species, the total weight loss due to vaporization is given by

$$\Delta w_{tot} = \sum_i \Delta w_i = \sum_i p_i[M_i/2\pi RT]^{1/2} taC \quad (3)$$

Substituing for p_i from Equation (1) and rearranging, we get

$$\Delta w_{tot} = \sum_i Q_i A_i \quad (4)$$

where

$$Q_i = [k/\sigma sh]_i[M_i/2\pi R]^{1/2} taC \quad (5)$$

and

$$A_i = \sum_T \int_t I_i T^{1/2}\, dt \quad (7)$$

For a sample vaporizing predominantly as two species

(referred to as 1 and 2) the equations can be modified to be

$$w_{tot}=Q_1[A_1+A_2r_2\{M_2/M_1\}^{1/2}] \quad (7)$$

where $r_2=(\sigma sh)_1/(\sigma sh)_2$.

From the total weight loss during the experiment and the respective A_i values, the unknown Q_1 can be calculated. Emplloying this method, the mass loss due to effusion of the individual gaseous species at any time during the vaporization experiment can be calculated. Subsequently, with a knowledge of the initial composition and mass of the sample used in the experiment, the composition at any point can be derived from the A_i values up to that time. Similar expressions can be written for cases where more than two species are evaporating.

RESULTS AND DISCUSSION

Vapour phase composition and determination of partial pressures

Table 1 gives the species detected in the mass spectrum of the equilibrium vapour of various metal–tellurium samples studied. It is seen that when the condensed phase consisted of metal telluride, the mass spectrum mainly consisted of Te^+ and Te_2^+ and no metal-bearing species could be detected. The exception is the Mn–Te system where both Mn^+ and Te^+ were detected. The mass spectrum has also shown the presence of Te_3^+ in the case of studies with a tellurium-rich two-phase mixture ($FeTe_{1-x}+FeTe_{2-y}$) in the Fe–Te system. Figure 1 gives a typical set of ionization efficiency curves for Te^+ and Te_2^+ where both the species are formed due to simple ionization. In Figure 2 similar curves for Te^+, Te_2^+ and Te_3^+ are given. In this case while Te_2^+ and Te_3^+ were formed due to simple ionization, Te^+ was formed due to fragmentation. Ionization efficiency curves for Mn^+ and Te^+ which are formed due to simple ionization are shown in Fig. 3. Appearance energies derived from the ionization efficiency curves are given in Table 1. The origin of the species, whether formed due to simple ionization (Reaction (8)) or fragmentation (Reaction (9)), was deduced by comparing the appearance energies with known first ionization energies. The first ionization energies of Te (9.0 eV) and Mn (7.6 eV) were taken from Moore's compilation.[19] Appearance energies for the formation of Te_2^+ and Te_3^+ were taken from References 20 and 21 respec-

Table 1. Species detected in the mass spectrum and the neutral species present in the equilibrium vapour

Sample[a]	Species detected in the mass spectrum[b]	Appearance energy (eV)[c]	Neutral species in the vapour phase[d]
$Fe+FeTe_{1-x}$	Te^+, Te_2^+	8.9, 8.3	Te, Te_2
$Ni+Ni_3Te_2$	Te^+, Te_2^+	9.3, 8.8	Te, Te_2
$Cr+CrTe_{1-x}$	Te^+, Te_2^+	9.0, 8.8	Te, Te_2
$Mo+Mo_3Te_4$	Te^+, Te_2^+	9.3, 8.8	Te, Te_2
Mn+MnTe	Mn^+, Te^+	7.6, 9.0	Mn, Te
$Mo_3Te_4+MoTe_2$	Te^+, Te_2^+	9.3, 8.8	Te, Te_2
$FeTe_{1-x}+FeTe_{2-y}$	Te^+, Te_2^+, Te_3^+	11.6, 9.0, 9.0	Te_2, Te_3

[a] The phases are nominally designated as in the respective recommended phase diagrams.
[b] The temperature range of measurement is given in Table 2.
[c] Appearance energies were derived by linear extrapolation of the ionization efficiency curves. An overall error of ±0.5 eV is estimated in the measured appearance energies. The values are listed in the same order as they are given in column 2 of this Table.
[d] Nature of the species, whether formed due to simple ionization or fragmentation, is concluded based on the agreement between measured appearance energies and the first ionization energies reported in the literature.

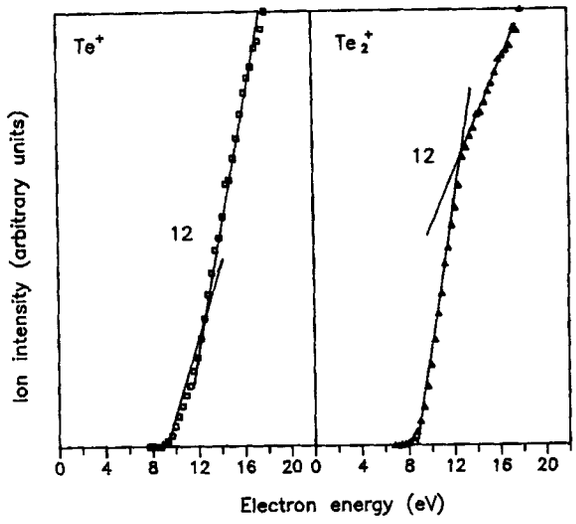

Figure 1. Ionization efficiency curves of Te^+ and Te_2^+. The data shown are recorded while studying the vaporization behaviour of ($Ni+Ni_3Te_2$) two-phase mixture.

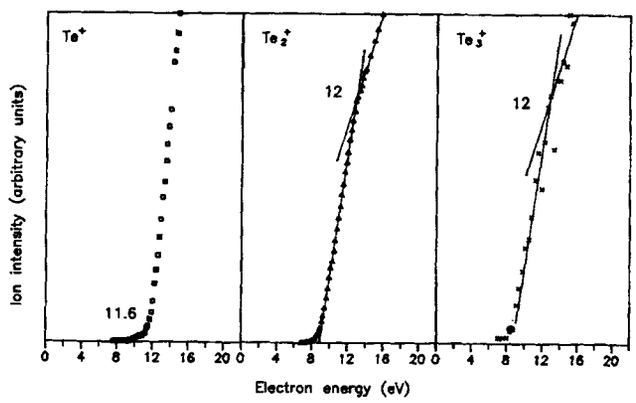

Figure 2. Ionization efficiency curves of Te^+, Te_2^+ and Te_3^+. The data shown are recorded while studying the vaporization behavior of the two-phase mixture ($FeTe_{1-x}+FeTe_{2-y}$).

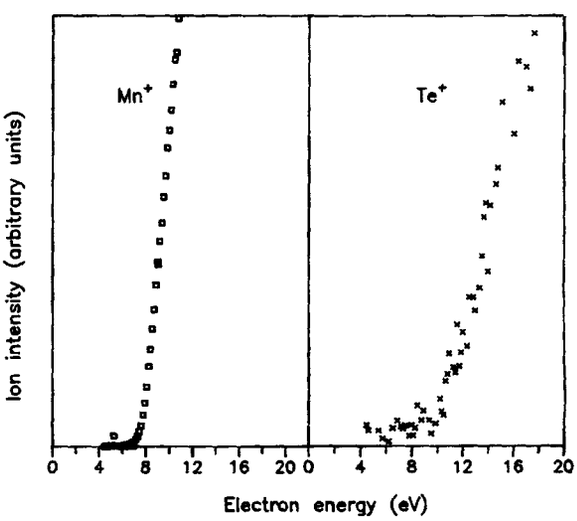

Figure 3. Ionization efficiency curves of Mn^+ and Te^+. The data shown are taken from studies with a (Mn+MnTe) two-phase mixture.

tively.

$$M_i + e = M_i^+ + 2e \text{ (simple ionization)} \quad (8)$$

$$M_i + e = M_{i-j}^+ + M_j + 2e \text{ (fragmentation)} \quad (9)$$

When the vapour phase consists of both the monomer and dimer of tellurium, the ion intensity at Te^+ can have a *contribution* due to the fragmentation of Te_2. For example, a change in the slopes of the ionization efficiency curves of Te^+ and Te_2^+ could be seen at an energy of ~12 eV (see Fig. 1). This is due to the fact that above this energy, Te^+ is formed both by simple ionization of Te(g) as well as fragmentation of Te_2(g). Similar changes in the slopes can be seen in the case of the ionization efficiency curves of Te_2^+ and Te_3^+ shown in Fig. 2. The ionization efficiency curve of Te^+ in Fig. 3 does not show any change in the slope because, in this case, Te^+ is formed only by simple ionization of Te(g). In the case where an ion is formed both by simple ionization and by fragmentation, the ion intensities measured at an electron energy less than the fragmentation energy were chosen for converting them into partial pressures. For example, ion intensities of Te^+ and Te_2^+ measured at energies <10 eV were generally chosen for deriving partial pressures in our studies. The choice of a low energy, where fragmentation cannot occur, avoids the need to correct for fragmentation. For the dimer of tellurium the value of k' was calculated directly from the ion intensities measured over pure tellurium at appropriate energies. The ratio of $\sigma(Te_i)/\sigma(Te_2)$ required to obtain $k'(Te_i)$, for other tellurium-bearing species, from $k'(Te_2)$ was calculated employing the following relation[3, 20, 22]

$$\sigma(Te_i) = \sigma(Te_2)(i/2)^{1/2} \quad (10)$$

For the measurements at energy E, lower than that corresponding to maximum ionization (E_{max}), the ionization cross section $\sigma(Te_i)_E$ is calculated using the relation suggested by Drowart[11]

$$\sigma(Te_i)_E = \sigma(Te_i)_{max}(E - E_A)(E_{max} - E_A) \quad (11)$$

where E_A is the appearance energy.

In the case of studies with (Mn+MnTe), the vapour phase was found to consist of predominantly Mn(g) and traces of Te(g). The instrument calibration constant (k'(Mn)) was obtained *in situ* from the measured ion intensities of Mn^+ and known partial pressures of manganese.[23] k'(Te) was calculated from k'(Mn) by using the relation

$$k'(Te) = k'(Mn)\{\sigma sh(Mn)/\sigma sh(Te)\} \quad (12)$$

The ionization cross sections for manganese and tellurium required for this purpose were taken from Mann's compilation.[24] Table 2 gives the partial pressure–temperature relations obtained for various two-phase mixtures studied by us. It is seen that amongst the various ($M+MTe_x$) two-phase mixtures, $p(Te_2)$ and p(Te) at 1000 K were found to be highest in the equilibrium vapour over the two-phase mixture ($Fe+FeTe_{1-x}$) and lowest for (Mn+MnTe). The variation of the partial pressures of Te(g), Te_2(g) and Te_3(g) as a function of temperature are shown in Figs 4, 5 and 6. In Figs 5 and 6, the p–T data of Te_2(g) and Te_3(g) of pure tellurium[17, 21] are also shown for comparison.

Determination of homogeneity ranges of non-stoichiometric metal tellurides

While the tellurides of Fe, Cr and Mo preferentially vaporize as tellurium, manganese telluride was found to vaporize as manganese. In the case of samples vaporizing preferentially as tellurium the starting composition consisted of either a two-phase mixture or a single phase of high tellurium activity. For example, in the case of determination of the homogeneity range of the $FeTe_{1-x}$ phase, the starting samples were a mixture of $FeTe_{1-x}$ and $FeTe_{2-y}$ phases. Table 3 gives the details of the phases that were present in the samples used for obtaining the homogeneity ranges both at the beginning and at the end of the vaporization experiments. Generally, samples of at least two different compositions (but still belonging to the same phase-field) were used in these homogeneity range experiments. The composition at the end of the experiment given

Table 2. Partial pressure–temperature relations over various two-phase metal tellurides

Phase field	Temperature range (K)	$\log[p_i/P_*] = -A/T(K) + B$ A	B	p_i/P_* at 1000 K
i=Te				
$Fe+FeTe_{1-x}$	901–1048	12 227±400	11.03±0.41	6.35×10^{-2}
$Ni+Ni_3Te_2$[a]	893–993	13 350±425	11.11±0.45	5.75×10^{-3}
$Ni+Ni_3Te_2$[b]	1020–1055	11 189±510	8.95±0.49	5.77×10^{-3}
$Ni+Ni_3Te_2$[b]	1090–1190	11 930±400	9.67±0.35	5.50×10^{-3}
$Cr+CrTe_{1-x}$	1015–1138	14 360±452	11.51±0.42	1.41×10^{-3}
$Cr+CrTe_{1-x}$[c]	1180–1285	13 091±533	10.44±0.43	2.23×10^{-3}
$Mo+Mo_3Te_4$	960–1110	13 238±116	11.67±0.11	2.70×10^{-2}
Mn+MnTe	1120–1250	16 099±285	10.53±0.24	2.70×10^{-6}
$Mo_3Te_4+MoTe_2$	820–950	14 120±196	13.01±0.22	7.76×10^{-2}
$i=Te_2$				
$Fe+FeTe_{1-x}$	885–1048	10 759±284	11.12±0.29	2.30
$Ni+Ni_3Te_2$[a]	893–993	12 563±223	10.95±0.24	2.44×10^{-2}
$Ni+Ni_3Te_2$[b]	1020–1055	10 883±461	9.31±0.44	2.67×10^{-2}
$Ni+Ni_3Te_2$[b]	1090–1190	11 187±344	9.65±0.30	2.90×10^{-2}
$Cr+CrTe_{1-x}$	1015–1138	14 894±408	12.00±0.38	1.28×10^{-3}
$Cr+CrTe_{1-x}$[c]	1180–1285	13 015±533	10.36±0.43	4.62×10^{-3}
$Mo+Mo_3Te_4$	960–1110	13 631±97	13.00±0.10	2.34×10^{-1}
$FeTe_{1-x}+FeTe_{2-y}$	659–759	11 341±97	13.92±0.14	3.67×10^{-1}[d]
$Mo_3Te_4+MoTe_2$	820–950	14 979±210	15.72±0.24	5.51
$i=Te_3$				
$FeTe_{1-x}+FeTe_{2-y}$	699–759	14 861±337	15.17±0.46	2.28×10^{-4}[d]

[a] Ni-rich Ni_3Te_2 phase.
[b] High temperature modification of Ni_3Te_2 phase.
[c] High temperature modification of $CrTe_{1-x}$ phase.
[d] The phase field ($FeTe_{1-x}+FeTe_{2-y}$) exists only below 792 K and hence $p(Te_i)$ given is at 790 K.

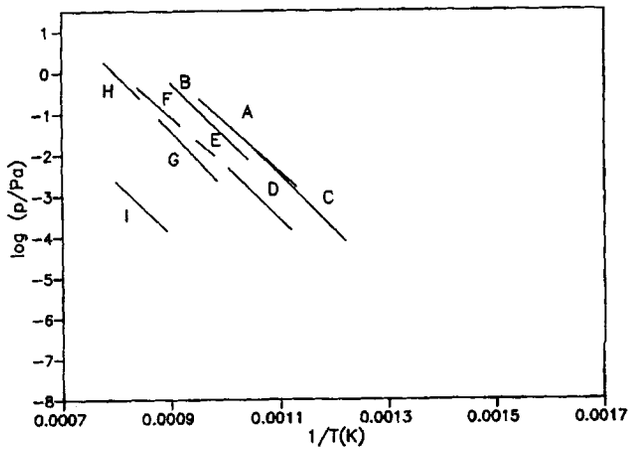

Figure 4. p(Te) as a function of temperature for various metal telluride phases. A, ($Fe+FeTe_{1-x}$); B, ($Mo+Mo_3Te_4$); C, ($Mo_3Te_4+MoTe_2$); D, ($Ni+Ni_3Te_2(NiTe_{0.63})$); E, ($Ni+Ni_3Te_2$) (high-temperature modification, $NiTe_{0.59}$); F, ($Ni+Ni_3Te_2$) (high temperature modification, $NiTe_{0.59}$); G, ($Cr+CrTe_{1-x}(CrTe_{1.03})$); *H*, ($Cr+CrTe_{1-x}$) (high temperature modification, $CrTe_{0.93}$) and I, (Mn+MnTe). Scaling of x, y axis was chosen to be the same for all the three Figures (Figs 4, 5 and 6) to enable direct comparison of partial pressures.

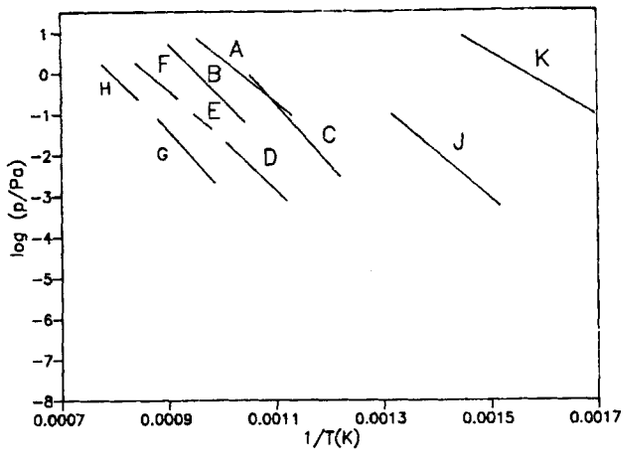

Figure 5. $p(Te_2)$ as a function of temperature for various metal telluride phases. A, $(Fe+FeTe_{1-x})$; B, $(Mo+Mo_3Te_4)$; C, $(Mo_3Te_4+MoTe_2)$; D, $(Ni+Ni_3Te_2(NiTe_{0.63}))$; E, $(Ni+Ni_3Te_2)$ (high temperature modification, $NiTe_{0.59}$); F, $(Ni+Ni_3Te_2)$ (high temperature modification, $NiTe_{0.59}$); G, $(Cr+CrTe_{1-x}(CrTe_{1.03}))$; H, $(Cr+CrTe_{1-x})$ (high temperature modification, $CrTe_{0.93}$) and J, $(FeTe_{1-x}+FeTe_{2-y})$. The $p°$ (Te_2) variation over pure Te(s) (curve K) is also shown for comparison.

in the Table is a typical value. Three types of boundary conditions were encountered in these vaporization experiments: (1) the sample is a two-phase mixture both at the beginning and at the end of the vaporization experiment (eg. Fe–Te, Mo–Te), (2) the starting composition corresponds to that of a single phase and the end composition to that of a two-phase mixture (e.g. Cr-rich Cr–Te alloys) and (3) the starting composition corresponds to a two-phase mixture and the end composition to a single phase (e.g. Mn–Te and Te-rich Cr–Te alloys). While the studies with Fe–Te, Mo–Te, Mn–Te and chromium-rich Cr–Te resulted in data for the homogeneity ranges of hitherto reported non-stoichiometric phases, in the case of tellurium-rich chromium tellurides, the existence of a new non-stoichiometric phase $CrTe_{4-y}$ (nominally designated by us)[6] could be detected.

The variation of ion intensity as a function of time in a typical experiment carried out to obtain the homogeneity range of the Mo_3Te_4 phase is shown in Fig. 7. Figure 8 shows a similar plot obtained in one of the homogeneity range experiments on $CrTe_{1-x}$. Since both Te(g) and Te_2(g) were present in the equilibrium vapour, ion intensities of

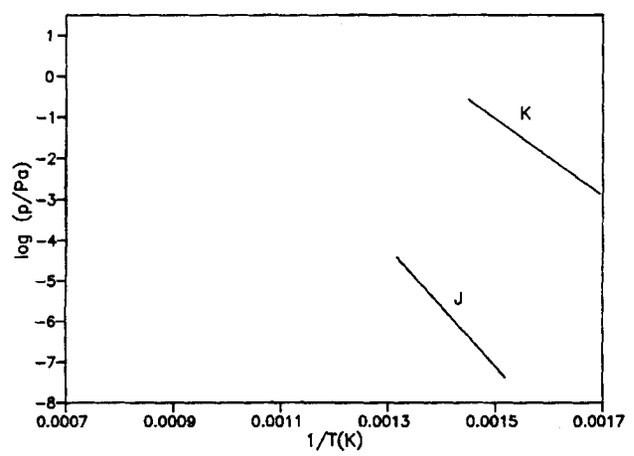

Figure 6. $p(Te_2)$ as a function of temperature for the two-phase field $(FeTe_{1-x}+FeTe_{2-y})$ (J). For comparison $p°$ (Te_2) vs T variation for Te(s) is also shown.

Table 3. Details of the phase compositions of the samples before and after the homogeneity range experiments

MTe_x Phase	T(K)	Composition of the sample (at% Te)[a] before[b]	after[c]	Co-existing phases in the sample before[b]	after[c]
$FeTe_{1-x}$	868	54.1	44.0	$FeTe_{1-x}+FeTe_{2-y}$	$Fe+FeTe_{1-x}$
$CrTe_{1-x}$	1075	55.6	50.9	$CrTe_{1-x}$	$Cr+CrTe_{1-x}$
		57.2	50.4	$CrTe_{1-x}$	$Cr+CrTe_{1-x}$
	1235	55.6	46.0	$CrTe_{1-x}$	$Cr+CrTe_{1-x}$
		57.2	45.1	$CrTe_{1-x}$	$Cr+CrTe_{1-x}$
Cr_5Te_8	650	80.0	62.0	$CrTe_{4-y}+Te$	Cr_5Te_8
		70.1	63.4	$Cr_5Te_8+CrTe_3$	Cr_5Te_8
		66.9	62.0	$Cr_5Te_8+CrTe_3$	Cr_5Te_8
$CrTe_3$	650	82.7	64.2	$CrTe_{4-y}+Te$	$Cr_5Te_8+CrTe_3$
		80.0	62.3	$CrTe_{4-y}+Te$	Cr_5Te_8
$CrTe_{4-y}$[d]	650	82.7	64.2	$CrTe_{4-y}+Te$	$Cr_5Te_8+CrTe_3$
		80.0	62.3	$CrTe_{4-y}+Te$	$Cr_5Te_8+CrTe_3$
Mo_3Te_4	950–975	60.6	51.2	$Mo_3Te_4+MoTe_2$	$Mo+Mo_3Te_4$
		62.6	52.9	$Mo_3Te_4+MoTe_2$	$Mo+Mo_3Te_4$
MnTe	1205–1280	40.1	44.3	Mn+MnTe	MnTe
		29.1	45.9	Mn+MnTe	MnTe

[a] A number of experiments were carried out with each composition of the sample. The composition at the end of the experiment given in the Table is a typical value.
[b] At the beginning of the homogeneity range experiment.
[c] At the end of the homogeneity range experiment.
[d] A new nonstoichiometric phase identified by us.[6]

both these species were followed as a function of time and are shown in Fig. 8. In the case of homogeneity-range experiments with (Mn+MnTe) alloys the sample became progressively poorer in manganese as the samples were found to be predominantly vaporizing as Mn(g). Te(g) was also found in the vapour phase but the ratio of p_{Mn} to that of p_{Te} was found to be 10^3. Figure 9 gives the ion intensity vs. time variation of Mn^+ and Te^+ in one such homogeneity-range experiment. Table 4 gives the homogeneity ranges and phase boundaries obtained for various metal tellurides studied by us. The recommended phase boundary compositions given in the Table are derived by taking the average of all the data obtained from all the experiments carried out with different initial compositions and at different temperatures) for a particular phase. Amongst the M-rich MTe_x phases, the MnTe phase was found to have the largest homogeneity range and that of $CrTe_{1-x}$ to be the smallest. The smallest homogeneity range was found in the case of $CrTe_{4-y}$ phase, the most tellurium-rich chromium telluride.

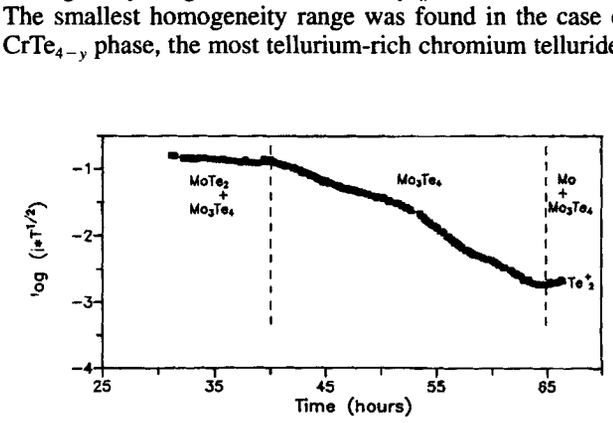

Figure 7. $\log(I(Te_2^+)T^{1/2})$ as a function of time at a constant temperature of 950 K. The sample initially consisted of the two-phase mixture $(MoTe_2+Mo_3Te_4)$. Owing to preferential evaporation of tellurium, the condensed phase became richer in Mo. The condensed phase composition changed from $(MoTe_2+Mo_3Te_4)$ to (Mo_3Te_4) to $(Mo+Mo_3Te_4)$ during the course of the experiment.

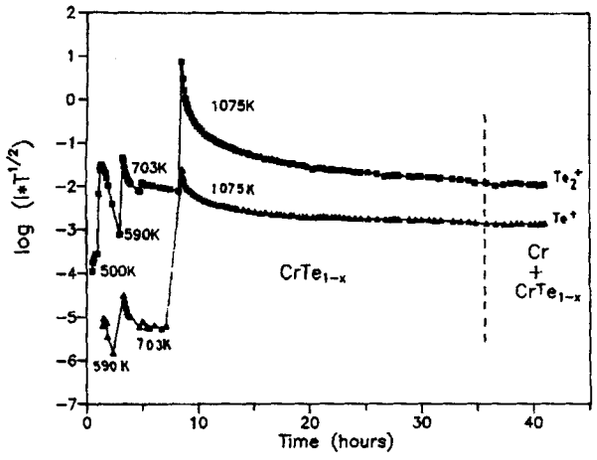

Figure 8. Variation of log ($IT^{1/2}$) as a function of time during the experiment carried out to determine the Cr-rich phase boundary of the most Cr-rich telluride. The starting composition is single phase $CrTe_{1-x}$ and due to preferential evaporation of tellurium the condensed phase became richer in chromium and finally the sample became a ($Cr+CrTe_{1-x}$) two-phase mixture.

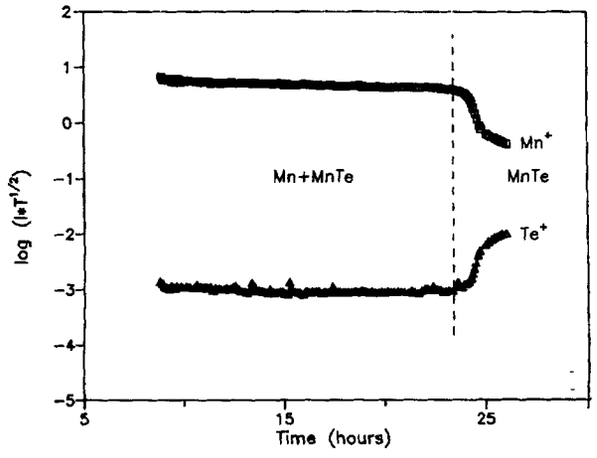

Figure 9. Weight loss experiments for the determination of the Mn-rich phase boundary of MnTe at 1250 K. Initially the sample was a two-phase mixture (Mn+MnTe). Due to preferential evaporation of Mn, the condensed phase became depleted in Mn and finally the sample became a single phase MnTe. Since both Mn and Te were present in the equilibrium vapour, the ion intensities of both these species were monitored and are shown in the Figure.

Table 4. Phase-boundary compositions of the non-stoichiometric metal telluride phases determined in the present study

System	Phase	T(K)	Homogeneity range (at % Te) M-rich	Te-rich	Formula M-rich	Te-rich
Fe–Te	$FeTe_{1-x}$	868	44.78	48.43	$FeTe_{0.81}$	$FeTe_{0.94}$
Cr–Te	$CrTe_{1-x}$	1075	50.72		$CrTe_{1.03}$	
		1235	48.25		$CrTe_{0.93}$	
	Cr_5Te_8	650	63.6		$CrTe_{1.75}$	
	$CrTe_3$	650	70.5	74.4	$CrTe_{2.39}$	$CrTe_{2.91}$
	$CrTe_{4-y}$	650	77.0	78.3	$CrTe_{3.35}$	$CrTe_{3.61}$
Mo–Te	Mo_3Te_4	950–975	52.4	56.5	$MoTe_{1.1}$	$MoTe_{1.3}$
Mn–Te	MnTe	1205–1280	44.3		$MnTe_{0.8}$	

Determination of thermodynamic quantities from partial pressure-temperature data

The general vaporization reaction can be represented as

$$MTe_x(s) = MTe_y(s) + ((x-y)/n)Te_n(g) \quad (13)$$

where $n=1$ for monomer, 2 for dimer and 3 for trimer and $y=0$ when the studies were carried out with ($M+MTe_x$) samples. Reaction enthalpies were determined by employing the Second and Third-Law methods:[11]

$$\Delta_r H_T^\circ = -R\{d\ln(K_p)/d(1/T)\}$$

(Second Law method) (14)

and

$$\Delta_r H_{298.15}^\circ = -T\{R\ln(K_p) + \Delta(G_T^\circ - H_{298}^\circ/T)\}$$

(Third-Law method) (15)

In the above expressions K_p refers to the equilibrium constant at temperature T for the reaction (for example for Reaction (13) the equilibrium constant $K_p = [p(Te_n))^{(x-y)/n)}]$. $\Delta_r H_T^\circ$ and $\Delta_r H_{298.15}^\circ$ refer to the enthalpy changes at T_m and 298.15 K respectively, T_m is the mean temperature and $(G_T^\circ - H_{298}^\circ)/T$ represents the Gibbs free energy function of the participants in the chemical reaction. The Second-Law enthalpies, $\Delta_r H_T^\circ$, were computed from the least-squares fitted slopes of the ln K_p vs $1/T$ plots. These data were converted to $\Delta_r H_{298.15}^\circ$ using the enthalpy increments $(H_T^\circ - H_{298}^\circ)$. The values thus obtained for various reactions are given in Table 5 along with reaction enthalpies obtained by the Third-law method. The required enthalpy increments and Gibbs free energy functions are either taken from the literature or estimated by us; the details can be found elsewhere.[2–9] Generally there is good agreement between the two, indicating the reliability of the measured partial pressures.

Enthalpies of formation of various metal-rich metal telluride phases were derived by taking the enthalpy of the following reaction

$$2\,Te(s) = Te_2(g) \quad (16)$$

The enthalpy for this reaction was also obtained by us from studies on the vaporization behaviour of pure tellurium.[17,21] The Gibbs free energy of formation was obtained by using the relation

$$\Delta_f G_{298.15}^\circ = \Delta_f H_{298.15}^\circ - T\left(\sum_{\text{products}} S_{298.15}^\circ - \sum_{\text{reactants}} S_{298.15}^\circ\right) \quad (17)$$

When the reaction involves more than one metal telluride, the enthalpy and Gibbs free energy of formation of one of the telluride phases is required to derive thermodynamic data for the other phase. For example, enthalpy of Reaction (18)

$$FeTe_{1.99}(s) = FeTe_{0.94}(s) + 0.525\,Te_2(g) \quad (18)$$

is given by $\Delta_r H_m^\circ = \Delta_t H_m^\circ(FeTe_{0.94}) + 0.525\,\Delta_f H_m^\circ(Te_2) - \Delta_f H_m^\circ(FeTe_{1.99})$. Hence to obtain the enthalpy of formation of the $FeTe_{1.99}$ phase, from the enthalpy of the reaction, a prior knowledge of the enthalpy of formation of $FeTe_{0.94}$ is necessary. Thermodynamic data for the phases $FeTe_{0.94}$ and $MoTe_{1.3}$ derived from the present study were used for deriving the enthalpy and Gibbs free energy of formation of $FeTe_{2-y}$ and $MoTe_2$.

Partial pressures of $Te_2(g)$ were determined as a function of composition in the experiments carried out to obtain the homogeneity range of the non-stoichiometric phases (eg.

Table 5. Second and Third Law enthalpies of reactions involving metal tellurides determined in the present work

System	Reaction	$\Delta_f H^\circ_m$ at 298.15 K in kJ/mol Second Law[b]	Third Law[b]	recommended[c]
Fe–Te	$FeTe_{0.8}(s)=Fe(s)+0.4\ Te_2(g)$	89.0±3.2	83.7±0.6	86.3±3.6
	$FeTe_{0.8}(s)=Fe(s)+0.8\ Te(g)$	193.8±3.7	187.5±1.3	190.7±4.3
	$FeTe_{1.99}(s)=FeTe_{0.94}(s)+0.525\ Te_2(g)$	117.0±2.7	131.1±0.5	124.1±10.3
	$FeTe_{1.99}(s)=FeTe_{0.94}(s)+0.35\ Te_3(g)$	103.3±4.0	117.8±0.3	110.6±10.9
Ni–Te[a]	$NiTe_{0.63}(s)=Ni(s)+0.315Te_2(g)$	84.1±3.7	81.0±0.4	82.6±3.0
	$NiTe_{0.63}(s)=Ni(s)+0.63Te(g)$	164.6±6.4	163.1±3.4	163.9±4.6
Cr–Te	$CrTe_{1.03}(s)=Cr(s)+0.515Te_2(g)$	154.2±5.1	150.0±1.6	152.1±6.9
	$CrTe_{1.03}(s)=Cr(s)+1.03Te(g)$	288.9±5.6	282.1±2.3	285.5±11.6
Mo–Te	$MoTe_{1.1}(s)=Mo(s)+0.55Te_2(g)$	153.6.±4.3	153.6±0.5	153.3±4.7
	$MoTe_{1.1}(s)=Mo(s)+1.10Te(g)$	291.8±8.2	291.9±1.0	291.8±11.0
	$MoTe_{1.89}(s)=MoTe_{1.3}(s)+0.295Te_2(g)$	91.0±3.9	78.1±0.7	84.6±10.6
	$MoTe_{1.89}(s)=MoTe_{1.3}(s)+0.59Te(g)$	166.9±6.4	154.6±0.9	160.7±13.6
Mn–Te	$MnTe_{0.8}(s)=Mn(s)+0.8\ Te(g)$	256.9±16.0	251.7±1.1	254.4±15.1

[a] Nickel-rich Ni_3Te_2 phase.
[b] The errors quoted are standard deviations of the mean of the data obtained for several runs.
[c] The recommended value is the average of the Second and Third Law values.

the $FeTe_{1-x}$, Mo_3Te_4 and $CrTe_{1-x}$ phases). These experiments, apart from allowing us to delineate the phase boundaries, also yielded the chemical potential of tellurium across the homogeneity range. The chemical potential of the other component (M in MTe_x) was calculated using Gibbs–Duhem integration. The value for a_M at one of the phase boundary compositions required for such a calculation was either taken to be equal to 1 (e.g. $(Fe+FeTe_{1-x})$[3] and $(Mo+Mo_3Te_4)$[8] or taken from the literature (e.g. $(CrTe_{4-x}+Te)$.[6]) Table 6 gives the compilation of thermodynamic data derived for various metal tellurides in the present work. The thermodynamic data indicate that it is the manganese telluride which is most stable, while that of iron is the least stable.

Since the vapour phase of most of the telluride phases studied consisted of both monomeric and dimeric tellurium species, the gas-phase dissociation constant for the reaction

$$Te_2(g)=2Te(g) \qquad (19)$$

could also be derived, based on the partial pressures determined. The temperature dependence of the equilibrium constant for Reaction 19 could be derived over the temperature range 820–1285 K.[25] The least-square fitted data of K_p $[p(Te)^2/p(Te_2)]$ vs. temperature is given by the following equation

$$\log(K_p)=-13\,892/T(K)+11.069 \qquad (20)$$

This is the first time that such an equation could be obtained based on experimental data covering such a wide temperature range. The Third Law enthalpy of dissociation obtained by taking all the data points into consideration gave a value of 257.6±4.1 kJ/mol which is in excellent agreement with those values derived based on photoionization (260.7±2.1 kJ/mol)[20] and spectroscopy (253.3±1.2 kJ/mol).[26]

Calculation of threshold tellurium potential required for the formation of cladding component tellurides

The threshold tellurium potential required for the formation of metal tellurides from stainless steel (ss) cladding could be calculated by considering the following reaction

$$[M]_{ss}+Te(s,1)=MTe_x(s) \qquad (21)$$

The activity of stainless steel constituents[27] and the partial pressure data over liquid tellurium[28] required for this purpose were taken from the literature. Such data calculated

Table 6. Enthalpy and Gibbs free energy of formation (in kJ/mol) of metal tellurides

System	Phase	M-rich formula	$\Delta_f H^\circ_m$	$\Delta_f G^\circ_m$	Te-rich formula	$\Delta_f H^\circ_m$	$\Delta_f G^\circ_m$	T(K)[a]
Fe–Te	$Fe-Te_{1-x}$	$FeTe_{0.81}$	−17.2	−21.1	$FeTe_{0.94}$	−27.8	−29.7	298.15
	$FeTe_{2-y}$	$FeTe_{1.99}$	−65.8	−58.3				298.15
Ni–Te	Ni_3Te_2	$NiTe_{0.63}$	−33.3	−35.0				298.15
		$NiTe_{0.59}$[b]	−27.7	−30.1				1038.15
		$NiTe_{0.59}$[b]	−30.5	−30.7				1140.00
Cr–Te	$Cr-Te_{1-x}$	$CrTe_{1.03}$	−68.1	−70.3				298.15
		$CrTe_{0.93}$[c]	−65.2	−55.7				1232.50
	Cr_5Te_8				$CrTe_{1.75}$		−86.2	650.00
	$CrTe_3$	$CrTe_{2.91}$		−90.4	$CrTe_{2.39}$		−89.5	650.00
	$CrTe_{4-y}$	$CrTe_{3.35}$		−90.5	$CrTe_{3.61}$		−90.7	650.00
Mo–Te	Mo_3Te_4	$MoTe_{1.1}$	−63.7	−65.1	$MoTe_{1.3}$	−67.0		298.15
					$MoTe_{1.3}$		−54.6	950.00
	$MoTe_2$	$MoTe_{1.89}$	−105.8	−101.6				298.15
Mn–Te	MnTe	$MnTe_{0.8}$	−86.8	−90.0				298.15

[a] The reference states were taken to be the respective elements in their standrd states i.e. M(s) and Te(s). Whenever the temperature was >726 K the reference state for tellurium was taken to be Te(I).
[b] High temperature modification of Ni_3Te_2 phase.
[c] High temperature modification of $CrTe_{1-x}$ phase.

Table 7. Threshold tellurium potential required for the formation of cladding component tellurides and the equilibrium tellurium potential that is likely to exist in the fuel–cladding gap

Equilibria	M in MTe_x[b]	O/M of the fuel[c]	$\Delta\bar{G}_{Te}$(kJ/mol) at 1000 K	1100 K
$[M]_{ss}$[a]/MTe_x				
	Mo		−17.4	−6.3
	Fe		−30.7	−29.6
	Ni		−44.9	−46.2
	Cr		−54.0	−50.6
	Mn		−71.4	−72.8
$Cs_2Te/MO_{2+x}/Cs_2Mo_4$[d]				
		1.9998	−233.1	−215.5
		2.0000	−120.2	−121.0
		2.0002	−7.3	−26.6

[a] ss: stainless steel.
[b] $x=0.81$ for Fe–Te; $x=1.03$ up to 1160 K and 0.93 above 1160 K for Cr–Te; $x=0.63$ up to 1010 K and 0.59 above 1010 K for Ni–Te; $x=1.1$ for Mo–Te, and $x=0.8$ for Mn–Te.
[c] O/M=1.9998: hypostoichiometric fuel; O/M=2.0000: stoichiometric fuel; O/M=2.0002: hyperstoichiometric fuel.
[d] $M=U_{0.75}Pu_{0.25}$

at two temperatures, namely 1000 and 1100 K, are given in Table 7. In order to assess the possibility of cladding attack in an oxide-fuelled fast-breeder reactor, the tellurium potential that is likely to exist in the fuel–cladding gap needs to be calculated. This was done by considering the following equilibrium

$$Cs_2Te(l)+MO_{2+x}(s)+[(2\pm x)/2]O_2(g)=Cs_2MO_4(s)+Te(l) \quad (22)$$

where $M=U_{0.75}Pu_{0.25}$. Equilibrium potentials calculated for three different fuels (namely hypo-stoichiometric, stoichiometric and hyper-stoichiometric) are also given in Table 7. The details of these calculations are given elsewhere:[5, 17, 29, 30] Two important conclusions could be drawn from these calculations (a) in the case of cladding attack by tellurium it is the manganese telluride which will be formed first and (b) only hyper-stoichiometric fuels possess a sufficient equilibrium tellurium potential to attack the clad.

CONCLUSION

In this paper we have summarized thermodynamic studies on metal–tellurium systems relevant to the understanding of fuel–cladding interaction for fast-reactor fuels. Partial pressure–temperature data and the homogeneity ranges of the non-stoichiometric metal telluride phases could be derived by employing Knudsen effusion mass spectrometry.

Acknowledgements

The authors wish to thank members of the mass spectrometric group, R. Balasubramanian, D. Darwin Albert Raj and T. S. Lakshmi Narasimhan who have contributed significantly to this work. The authors also wish to thank K. C. Srinivas, R. Parthasarathi and B. Suhasini of the electronics and instrumentation group for carrying out various modifications to the mass spectrometer.

REFERENCES

1. M. G. Adamson, E. A. Aitken and T. B. Lindemaier, *J. Nucl. Mater.* **130**, 375 (1985).
2. B. Saha, R. Viswanathan, M. Sai Baba, D. Darwin Albert Raj, R. Balasubramanian, D. Karunasagar and C. K. Mathews, *J. Nucl. Mater.* **130**, 316 (1985).
3. M. Sai Baba, R. Viswanathan, R. Balasubramanian, D. Darwin Albert Raj, B. Saha and C. K. Mathews, *J. Chem. Thermodyn.* **20**, 1157 (1988).
4. R. Viswanathan, M. Sai Baba, D. Darwin Albert Raj, R. Balasubramanian, B. Saha and C. K. Mathews, *J. Nucl. Mater.* **149**, 302 (1987).
5. R. Viswanathan, M. Sai Baba, D. Darwin Albert Raj, R. Balasubramanian, B. Saha and C. K. Mathews, *J. Nucl. Mater.* **167**, 94 (1989).
6. R. Viswanathan, M. Sai Baba, T. S. Lakshmi Narasimhan, R. Balasubramanian, D. Darwin Albert Raj and C. K. Mathews, *J. Alloys and Compounds* **206**, 201 (1994).
7. R. Viswanathan, R. Balasubramanian and C. K. Mathews, *J. Chem. Thermodyn.* **21**, 1183 (1989).
8. R. Viswanathan, D. Darwin Albert Raj, T. S. Lakshmi Narasimhan, R. Balasubramanian and C. K. Mathews, *J. Chem. Thermodyn.* **25**, 533 (1993).
9. M. Sai Baba, T. S. Lakshmi Narasimhan, R. Balasubramanian and C. K. Mathews, *J. Nucl. Mater.* **201**, 147 (1993).
10. J. L. Margrave, *Characterisation of high-temperature vapors and gases*, National Bureau of Standards, Special publication 561/1 and 561/2, U.S. Government printing office, Washington, vol. 1 and 2.
11. J. Drowart in *Mass Spectrometry and High Temperature Chemistry, Proc. Int. School on Mass Spectrom.*, Jozef Stefan Institute, Lubljana, Slovenia, 1969, J. Marsel (Ed.) (1971) p. 187.
12. K. A. Gingerich in *Current Topics in Materials Science*, Vol. 6, Kaldis, (Ed.) North Holland, Amsterdam, 1980, p. 345.
13. K. Hilpert, in *Structure and Bonding 73*, Springer-Verlag, Berlin, 1990, p. 97.
14. M. Sai Baba, T. S. Lakshmi Narasimhan, R. Balasubramanian and C. K. Mathews, *Int. J. Mass Spectrom. Ion Processes* **114**, R1 (1992).
15. M. Sai Baba, T. S. Lakshmi Narasimhan, R. Balasubramanian and C. K. Mathews, *J. Phys. Chem.* **99**, 3020 (1995).
16. *Radiochemistry Program Progress Report for the period 1980 and 1981*, Reactor Research Centre, Kalpakkam, India, 1982.
17. R. Viswanathan, Ph.D. Thesis, University of Madras, India (1991).
18. M. Sai Baba, Ph.D. Thesis, University of Madras, India (1995).
19. C. E. Moore, *Ionisation potentials and ionisation limits derived from the analysis of optical spectra*, National Bureau of Standards, US, NSRDS-NBS 1970 34.
20. J. Berkowitz and W. A. Chupka, *J. Chem. Phys.* **50**, 4245 (1969).
21. R. Viswanathan, M. Sai Baba, D. Darwin Albert Raj, R. Balasubramanian and C. K. Mathews, in *Advances in Mass Spectrometry*, J. F. J. Todd (Ed.), 13B, p. 1087, Wiley, Chichester, 1986.
22. R. Viswanathan, M. Sai Baba, D. Darwin Albert Raj, R. Balasubramanian and C. K. Mathews, *Proceedings of Third National Symposium on Mass Spectrometry — Research Application and Instrumentation*, Hyderabad, 1985 (Indian Society for Mass Spectrometry, Bombay, 1986), A7.
23. C. B. Alcok, V. P. Itkin and M. K Horrigan, *Canadian Metall. Quart.* **23**, 309 (1984).
24. J. B. Mann, *Proc. Int. Conf. on Mass Spectrometry*, 1970, K. Ogata and T. Hayakawa (Eds.), p. 814.
25. R. Viswanathan, M. Sai Baba, D. Darwin Albert Raj, R. Balasubramanian, T. S. Lakshmi Narasimhan and C. K. Mathews, *Spectrochimica Acta* **49B**, 243 (1994).
26. J. Verges, C. Effantin, O. Babaky, J. d'Inkan, S. J. Prosser and R. F. Barrow, *Phys. Scr.* **25**, 338 (1982).
27. A. M. Azad, O. M. Sreedharan and J. B. Gnanamurthy, *J. Nucl. Mater.* **144**, 94 (1987).
28. F. Gronvold, J. Drowart and E. F. Westrum Jr, *The Chemical Thermodynamic properties of Actinide Elements and Compounds, Part 4: The Actinide Chalcogenides* (excluding Oxides), (IAEA, Vienna, 1984).
29. B. Saha, R. Viswanathan, M. Sai Baba and C. K. Mathews, *High Temp–High Press*, **20**, 47 (1988).
30. C. K. Mathews, *J. Nucl. Mater.* **201**, 99 (1993).